EPR Studies on Molecular Orientation in a Surface-Stabilized Paramagnetic Liquid Crystal Cell

Yohei Noda,*,† Satoshi Shimono,† Masaaki Baba,† Jun Yamauchi,† Naohiko Ikuma,‡ and Rui Tamura‡

Graduate School of Science, Kyoto University, Kyoto 606-8502, and
Graduate School of Global Environmental Studies, Kyoto University, Kyoto 606-8501

Received: June 20, 2006; In Final Form: August 31, 2006

By EPR spectroscopy, we have developed a new method for determining the molecular orientation in a surface-stabilized liquid crystal (LC) cell, which includes a paramagnetic LC, (2*S*,5*S*)-2,5-dimethyl-2-heptyloxyphenyl-5-[4-(4-octyloxybenzenecarbonyloxy)phenyl]pyrrolidine-1-oxy (**1**), whose spin source is fixed in the rigid core. For each phase of racemic [(±)] and enantiomerically enriched [(*S*,*S*)] **1** in a surface-stabilized LC cell (4 μm thickness), the observed *g*-value profiles depending on the angle between the applied magnetic field and the cell plane were successfully simulated by the orientation models: (i) the LC molecule in the nematic (N) phase of (±)-**1** freely rotates around the long axis, which is always parallel to the rubbing direction; (ii) the long axis of the freely rotating LC molecule in the chiral nematic (N*) phase of (*S*,*S*)-**1** is always parallel to the cell plane but rotates in the plane to form a helical superstructure; and (iii) in the crystalline phase of (*S*,*S*)-**1**, the molecular long axis forms a helical superstructure similar to that of the N* phase, but the molecule is fixed around the long axis so that the NO bond lies in the cell plane. Fitting the temperature profile of the *g*-value in the N phase of (±)-**1** by use of the Haller equation, we determined the molecular *g*-values along the molecular long axis ($g_{||M}$) and short axis ($g_{\perp M}$), which were successfully reproduced by the use of the set of principal *g*-values of a similar nitroxide with consideration of the structure of the LC molecule optimized by Molecular Mechanics 3 (MM3).

Introduction

Aiming at hybrid orientation control by both electric and magnetic fields, a number of paramagnetic liquid crystals (LCs) have been synthesized.[1−5] To realize paramagnetism, there are two candidates for the spin source: d- or f-metal complexes and organic free radicals. Thus far, the former metallomesogens have been prepared intensively.[1−4] However, mesogens composed of metal complexes generally have high viscosities and high LC temperatures, which are unfavorable for the orientation control by external magnetic fields. To avoid these disadvantages, we have synthesized the all-organic chiral paramagnetic LC **1** (Figure 1).[5] **1** has a nitroxyl group fixed in the rigid core as a spin source, which is advantageous for orientation control by a magnetic field and can serve as the spin label or probe for the EPR investigation of the orientation of LC molecules. Although an EPR study of **1** in the bulk state has been reported,[5] the study of the oriented sample is expected to yield more detailed information.

By the use of a surface-stabilized LC cell, the orientation-controlled state of LC molecules can be obtained. Surprisingly, no EPR studies in the orientation-controlled state have been conducted using such an LC cell. By the use of an orientation-controlled sample, we can determine the Hamiltonian parameters as a tensor. Tensor information is less ambiguous and more useful than scalar information for decisive discussion.

The EPR study of the LC yields the parameters averaged through time and ensemble. The order parameter is useful for expressing the fluctuation from the director, that is, the average orientation of LC molecules. For the purpose of determining the order parameter, we measured the temperature profile of the *g*-value and fitted it by use of the Haller equation.

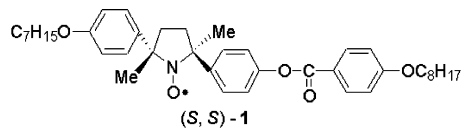

Figure 1. Molecular structure of the paramagnetic LC **1**.

Experimental Section

We prepared (±)- and (*S*,*S*)-**1** as reported previously (Figure 1).[5] The phase sequences of the samples are as follows: crystal−(63.3 °C)−N−(103.1 °C)−isotropic for (±)-**1** and crystal−(79.3 °C)−N*−(103.5 °C)−isotropic for (*S*,*S*)-**1**, where N and N* denote the nematic and chiral nematic phases, respectively. We used a commercially available thin-sandwich LC cell (EHC Co., Japan; 4 μm thickness) that consists of two indium tin oxide-coated glass plates covered with rubbed polyimide films. The cell gap was maintained by inserting 4-μm-thick spacers between the two plates. (±)- or (*S*,*S*)-**1** was filled into the cell gap in the isotropic phase by capillary action under vacuum, and then the cell was cooled to room temperature. As shown in Figure 2a, the cell size was 25 mm × 12 mm, and the rubbing directions on the top and the bottom planes were opposite (antiparallel configuration). To obtain the two-axis rotation data, we used two types of cells with different rubbing directions that were orthogonal to each other. As shown in Figure 2a, we defined one as a vertically rubbed cell and the other as a horizontally rubbed cell.

* To whom correspondence should be addressed. E-mail: nouda@t02.mbox.media.kyoto-u.ac.jp.
† Graduate School of Science.
‡ Graduate School of Global Environmental Studies.

10.1021/jp063836i CCC: $33.50
Published on Web 10/26/2006

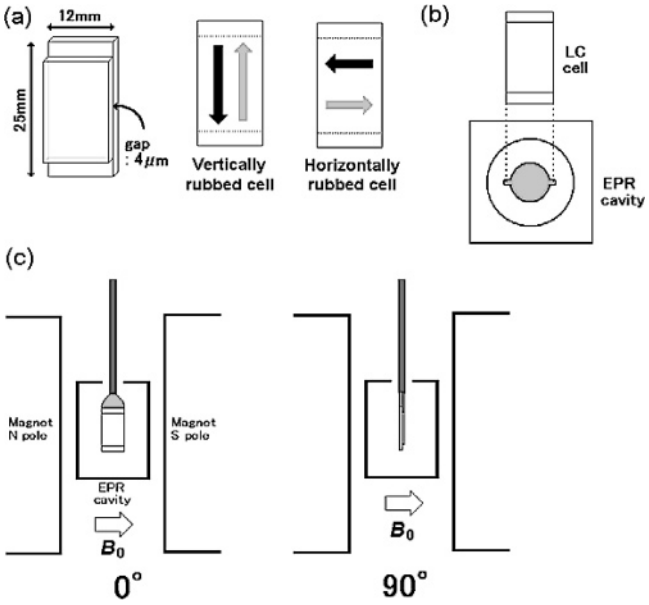

Figure 2. (a) (left) LC cell appearance and (middle and right) vertically and horizontally rubbed cells. The black and gray arrows indicate the rubbing direction of the top and bottom planes, respectively. (b) Top view of the EPR cavity, which was designed for the insertion and rotation of the LC cell. (c) Definition of the rotation angles of the LC cell to the applied magnetic field.

We used an EPR spectrometer (X-band, JEOL-FE1XG) whose cavity hole was modified for LC cell insertion (Figure 2b). The modification of the insertion hole did not cause a critical loss of the *Q*-factor. We measured the EPR spectrum at each angle by rotating the rod to which the LC cell attaches. The angle was defined as 0° when the cell plane was parallel to the applied static magnetic field (Figure 2c). We constructed a temperature control system, in that the sample was heated by the air flow. The system has two thermocouples: one is for monitoring the temperature near the heater, and the other is for monitoring the temperature near the LC cell. The temperature inhomogeneity in the cell area was estimated to be less than 1.5 deg.

Results and Discussion

We measured the angular dependence of the EPR spectrum for each phase of (±)- and (*S*,*S*)-**1**. The observed EPR spectra were fitted well by a single Lorentzian curve except for the crystalline phase of (±)-**1**, whose analysis has not yet been successful because of the complex waveform and poor reproducibility, which are most likely due to the coexistence of many crystal domains. Therefore, we analyzed the following five phases: the N and isotropic phases of (±)-**1** and the crystalline, N*, and isotropic phases of (*S*,*S*)-**1**. We obtained the *g*-value by referring to the peak position of the standard marker of Mn^{2+}/MgO. The results indicated that the isotropic phase exhibited a constant *g*-value (2.00655 ± 0.00005), which is independent of the angle. The N phase of (±)-**1** and the N* and crystalline phases of (*S*,*S*)-**1** showed characteristic angular profiles (Figure 3).

For the N phase of (±)-**1**, the angle profile of the vertically rubbed cell (○) was flat, while that of the horizontally rubbed cell (▲) oscillated significantly (Figure 3a). In contrast, for the N* and crystalline phases of (*S*,*S*)-**1**, the angle profiles of both rubbed cells were almost identical (Figure 3b and c). These experimental results can be explained by the orientation models shown in Figure 5. First, we must keep in mind that an LC molecule rotates around its molecular long axis in the N and the N* phases. We define $g_{||M}$ as the molecular *g*-value observed when the magnetic field is applied parallel to the long axis of the LC molecule and $g_{\perp M}$ as the molecular *g*-value observed when the magnetic field is applied orthogonally to the long axis (Figure 4b). Then, the *g*-value of the isotropic liquid phase (g_{iso}) is written as

$$g_{iso} = (g_{||M} + 2g_{\perp M})/3 \quad (1)$$

under the conditions of no orientation polarization by an external magnetic field. In the LC phase, the rotation axis fluctuates from the director (the average direction of the molecular long axis). To take this fluctuation into account, we define $g_{||}$ as the ensemble *g*-value observed when the magnetic field is applied parallel to the director and $g_{\perp}$ as the ensemble *g*-value observed when the magnetic field is applied orthogonally to the director (Figure 4a). Using the order parameter (*S*), we can write the relationship between the molecular and ensemble *g*-values:

$$g_{||} = g_{iso} + S(g_{||M} - g_{iso}), \quad g_{\perp} = g_{iso} + S(g_{\perp M} - g_{iso}) \quad (2)$$

Then, the relationship among $g_{||}$, $g_{\perp}$, and g_{iso} is written as

$$g_{iso} = (g_{||} + 2g_{\perp})/3 \quad (3)$$

under the conditions of no orientation polarization by an external field.

We now discuss the orientation models that explain the observed angular dependence of the *g*-value. The orientation

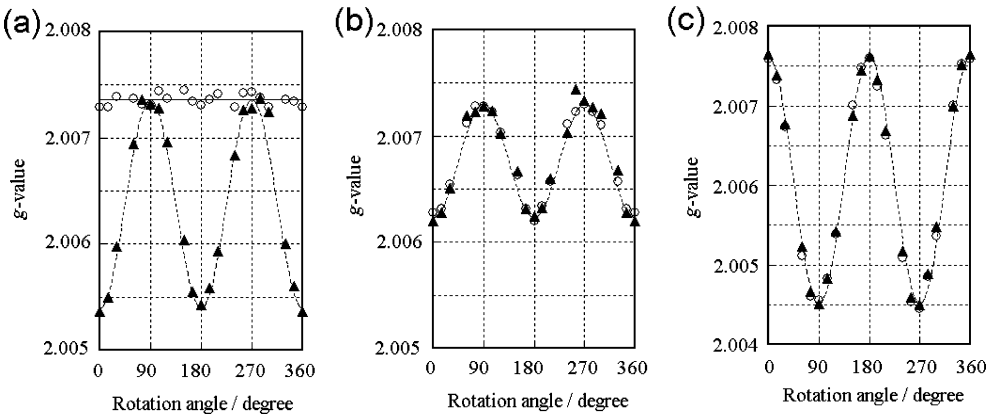

Figure 3. Angular dependence of the *g*-value for (a) the N phase of (±)-**1**, (b) the N* phase of (*S*,*S*)-**1**, and (c) the crystalline phase of (*S*,*S*)-**1**. The definition of the angle is shown in Figure 2c. White circles (○) and black triangles (▲) indicate the *g*-values for the vertically and horizontally rubbed cells, respectively.

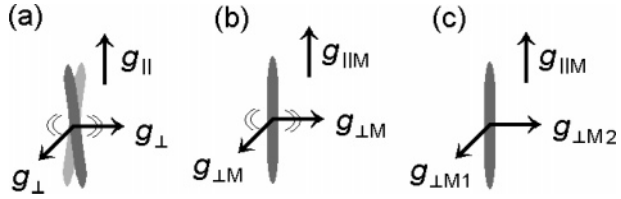

Figure 4. Schematic representation of the defined *g*-values: $g_{||}$, $g_{\perp}$, $g_{||M}$, $g_{\perp M}$, $g_{\perp M1}$, and $g_{\perp M2}$. (a) For a rotating LC molecule whose long axis is fluctuated from the director, we use $g_{||}$ and $g_{\perp}$. (b) For a rotating LC molecule whose long axis is perfectly aligned with the director, we use $g_{||M}$ and $g_{\perp M}$. (c) For a fixed LC molecule, we use $g_{||M}$, $g_{\perp M1}$, and $g_{\perp M2}$. The gray rods indicate the LC molecule. The double arcs drawn at both sides of the gray rod indicate the rotatory motion of the LC molecule.

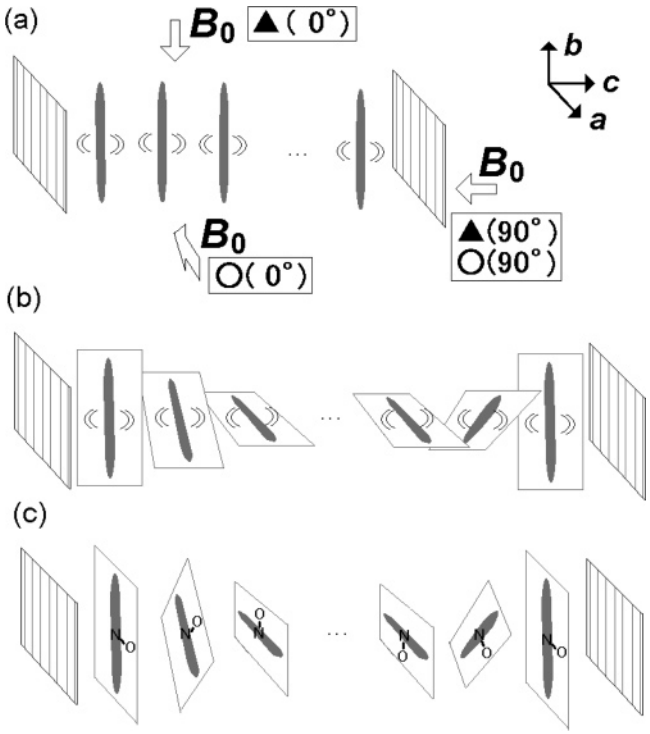

Figure 5. Orientation models of LC molecules in an LC cell for (a) the N phase of (±)-**1**, (b) the N* phase of (*S*,*S*)-**1**, and (c) the crystalline phase of (*S*,*S*)-**1**. The square planes on both sides indicate the LC cell surface, and the stripes on the cell surface indicate the rubbing direction. The gray rod indicates an LC molecule. The double arcs drawn on both sides of the gray rod indicate the rotatory motion of the LC molecule.

model for the N phase of (±)-**1** indicates that the LC molecule rotates around the long axis of the molecule, which is aligned with the rubbing direction on the cell surface, and that the direction of the long axis is uniform throughout the cell (Figure 5a). Since the angle between the magnetic field direction and the long axis of the molecule varies between 0 and 90° for the horizontally rubbed cell (▲), $g_{||}$ or $g_{\perp}$ is alternately observed. For the vertically rubbed cell (○), $g_{\perp}$ is observed constantly since the magnetic field is always orthogonal to the director.

The orientation model for the N* phase of (*S*,*S*)-**1** indicates that the LC molecule rotates around the long axis of the molecule, which aligns with the rubbing direction on the cell plane, and that the long axis between the two cell planes rotates to form a helical superstructure (Figure 5b). By the justification in the Supporting Information, the *g*-values observed for this model are obtained as follows:

$$g_a = (g_{||M} + g_{\perp M})/2, \quad g_b = (g_{||M} + g_{\perp M})/2, \quad g_c = g_{\perp M} \quad (4)$$

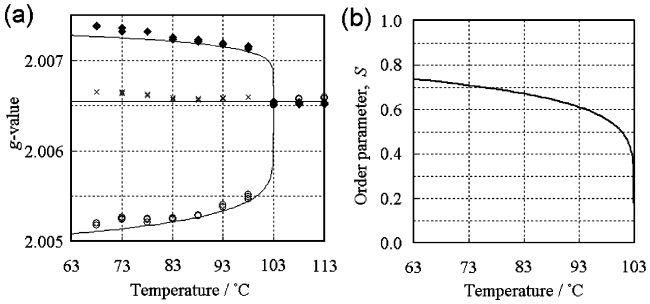

Figure 6. (a) Temperature dependence of the *g*-value of (±)-**1** in a horizontally rubbed cell. The white circles (○) indicate *g*-values of 0° ($g_{||}$). The black diamonds (◆) indicate *g*-values of 90° ($g_{\perp}$). The cross signs (×) indicate g_{ave} [$(g_{||} + 2g_{\perp})/3$]. The solid curve is calculated by the Haller equation. (b) Calculated curve of the order parameter, *S*.

where g_a, g_b, and g_c are the *g*-values observed when the magnetic field is parallel to the *a*, *b*, and *c* axes, respectively, as shown in Figure 5. Then, at the angle of 0°, g_a and g_b, which are observed for the vertically and horizontally rubbed cell, respectively, are identical, and at the angle of 90°, g_c is observed for both rubbed cells. The agreement between the angular profiles of both rubbed cells is due to the helical superstructure, whose helical axis is directed perpendicular to the cell plane.

Similar to the N* phase, the crystalline phase of (*S*,*S*)-**1**, which was obtained by cooling the N* phase, seems to retain the helical superstructure. In the crystalline phase, the LC molecule cannot rotate freely. We define $g_{\perp M1}$ and $g_{\perp M2}$ as the molecular *g*-value components that are within the normal plane of the molecular long axis and are orthogonal to each other (Figure 4c). By the justification in the Supporting Information, the *g*-values observed for this model are obtained as follows:

$$g_a = (g_{||M} + g_{\perp M1})/2, \quad g_b = (g_{||M} + g_{\perp M1})/2, \quad g_c = g_{\perp M2} \quad (5)$$

In this model, we set the direction of $g_{\perp M1}$ and $g_{\perp M2}$ as parallel and orthogonal to the cell plane, respectively. It is noteworthy that we use the molecular *g*-values, such as $g_{\perp M1}$, $g_{\perp M2}$, and $g_{||M}$, because LC molecules do not rotate in the crystalline phase. We will discuss later how the LC molecule is oriented around its long axis.

For the purpose of determining the molecular *g*-values ($g_{||M}$ and $g_{\perp M}$) by the use of the Haller equation, we measured the temperature dependence of the *g*-value in the N phase of (±)-**1**, which assumes the uniform orientation as shown thus far. The experiment was done for the horizontally rubbed cell (▲) at the angles of 0 and 90°, which correspond to $g_{||}$ and $g_{\perp}$, respectively (Figure 6a). Figure 6a also shows g_{ave} as defined:

$$g_{ave} = (g_{||} + 2g_{\perp}) \quad (6)$$

The obtained g_{ave} was approximately the same as g_{iso}, which is independent of the temperature. We performed the EPR measurement at a magnetic field of 0.33 T. If there is an orientation polarization induced by a magnetic field, the observed g_{ave} should deviate from g_{iso}. For example, in the case of a complete alignment of the molecular long axis to the applied magnetic field, the observed g_{ave} becomes the same as $g_{||}$. The agreement between g_{ave} and g_{iso} in the experimental result indicates that the magnetic field does not affect the molecular orientation. On the contrary, the bulk study showed that the molecular long axis is aligned with the magnetic field, as suggested by the *g*-value change from 2.0065 (crystalline phase) to 2.0052 (N phase) at the phase transition.[5] In the system of this study, the dominant source of orientation control is thought

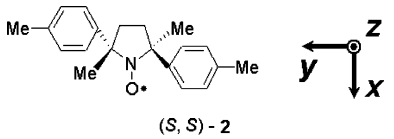

(*S*, *S*) - **2**

Figure 7. (left) Molecular structure of nitroxide **2**, which has a similar core structure to that of **1**. (right) Principal axes of the *g*-value.

to be the surface stabilization effect on the cell surface, which prevails over the magnetic field effect.

The temperature dependence of the *g*-value in the N phase follows the Haller equation:

$$g_{||}(T) = g_{||M}(1 - T/T^*)^{\beta} \qquad g_{\perp}(T) = g_{\perp M}(1 - T/T^*)^{\beta} \quad (7)$$

where T is the temperature (K), T^* is the transition temperature (K) between the N and isotropic phases, and β is the exponent parameter.[6,7] Applying $T = 0$ K to the theoretical curve of $g_{||}$ and $g_{\perp}$ gives us $g_{||M}$ and $g_{\perp M}$, respectively. We can then calculate the order parameter, S:

$$S(T) = (g_{||}(T) - g_{iso})/(g_{||M} - g_{iso})$$
$$S(T) = (g_{\perp}(T) - g_{iso})/(g_{\perp M} - g_{iso}) \quad (8)$$

We calculated the solid line curve in Figure 6a by assigning $g_{||M} = 2.00456$, $g_{\perp M} = 2.00754$, $T^* = 376$ K, and $\beta = 0.136$ to give the best fit with the experimental result. We then obtained the temperature profile of the order parameter S (Figure 6b).

We carried out another approach to obtain $g_{||M}$ and $g_{\perp M}$ by conducting a coordinate transformation on a set of principal *g*-values of a similar nitroxide into the molecular long axis frame, where the long axis of the LC molecule **1** corresponds to one of the sets of axes, while considering the structure of the LC molecule calculated by MM3. Fortunately, we obtained a set of the principal *g*-values for the nitroxide **2**, which has a similar core structure to that of **1** (Figure 7). The EPR study of the single crystal of **2** gave the principal *g*-values as $g_x = 2.00990$, $g_y = 2.00639$, and $g_z = 2.00266$,[8] where the subscripts *x*, *y*, and *z* indicate the principal axes, as shown in Figure 7. This set of principal *g*-values is thought to be valid by comparing them with known sets of the other five-member ring nitroxides, for example, $g_x = 2.0094$, $g_y = 2.0062$, $g_z = 2.0020$ for one case[9] and $g_x = 2.0101$, $g_y = 2.0068$, $g_z = 2.0022$ for another case.[10] However, the average of the principal *g*-values of **2** does not coincide with the g_{iso} of **1**. The *g*-value of a nitroxide shifts slightly depending on the molecular environment, such as the solvent polarity, and only g_x is sensitive to the environment, as previously shown theoretically[11,12] and experimentally.[13,14] In our study, the gap between g_{iso} of **1** and g_{ave} of **2** is most likely caused by the difference of the molecular environments, such as the distance between neighboring molecules. Such a difference should affect only g_x. Therefore, we adjusted the set of principal *g*-values by shifting g_x so that the average of the principal *g*-values becomes the same as g_{iso} of **1**. We then obtained this set of principal *g*-values: $g_x = 2.01060$, $g_y = 2.00639$, and $g_z = 2.00266$. In the following analysis, this set is used.

On the other hand, we calculated the molecular structure of **1** by MM3. In the optimized molecular structure, we defined the molecular long axis (z') as the line connecting the terminal C atoms of the alkyl chains of both sides. The unit vector of the molecular long axis is (0.04, 0.75, 0.66) in the principal axis coordinate system of the *g*-value. This shows that the molecular long axis is nearly orthogonal (92.4°) to the N−O bond but makes an angle of 41.4° with the C−N−C plane (Figure 8).

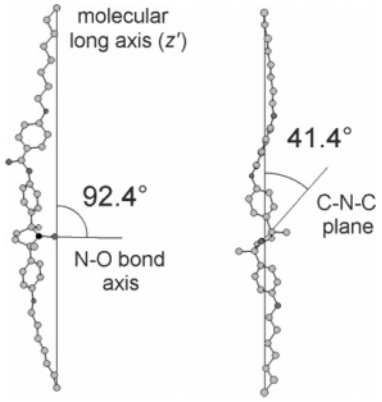

Figure 8. MM3-optimized molecular structure of **1**, showing the angles between the molecular long axis (z') and the principal axes of the nitroxide moiety. Carbon, oxygen, and nitrogen atoms are represented by light gray, dark gray, and black, respectively. Hydrogen atoms are omitted. The model on the right-hand side is obtained by rotating the model on the left-hand side by 90° around the vertical axis.

By the justification in the Supporting Information, the *g*-tensor for the LC molecule rotating around the molecular long axis (z') is represented as follows:

$$g = \begin{Bmatrix} (g_{x'x'} + g_{y'y'})/2 & 0 & 0 \\ 0 & (g_{x'x'} + g_{y'y'})/2 & 0 \\ 0 & 0 & g_{z'z'} \end{Bmatrix} \quad (9)$$

where $g_{x'x'}$, $g_{y'y'}$, and $g_{z'z'}$ are the *g*-tensor components along the x', y', and z' axes, respectively. The axes (x', y', and z') form the molecular long axis frame, where the z' axis corresponds to the molecular long axis and the two other axes (x' and y') are orthogonal to each other in the normal plane of the molecular long axis. We obtained the $g_{x'x'}$, $g_{y'y'}$, and $g_{z'z'}$ values by conducting a coordinate transformation on the set of principal *g*-values into the molecular long axis frame. Then, by applying the values of $g_{x'x'}$, $g_{y'y'}$, and $g_{z'z'}$ to eq 9, we obtained $(g_{x'x'} + g_{y'y'})/2 = 2.00744$ and $g_{z'z'} = 2.00477$. We then obtained $g_{||M} = 2.00477$ and $g_{\perp M} = 2.00744$ because $g_{||M} = g_{z'z'}$ and $g_{\perp M} = (g_{x'x'} + g_{y'y'})/2$ by the definition of the molecular *g*-values in the molecular long axis frame. These values are in good agreement with $g_{||M}$ and $g_{\perp M}$ obtained by the Haller fitting of the temperature-dependence experiment.

Finally, we discuss how the molecule orients around the long axis in the crystalline phase of (*S*,*S*)-**1**. For the following analysis, we employed a set of principal *g*-values described in the previous section, where $g_{||M} = 2.00477$ and $g_{\perp M} = 2.00744$. By applying $g_{\perp M1} = 2.01059$ and $g_{\perp M2} = 2.00429$, which is the case of maximum difference between $g_{\perp M1}$ and $g_{\perp M2}$, into eq 5, we achieved a good coincidence; the calculated values were $g_a = g_b = (g_{||M} + g_{\perp M1})/2 = 2.00768$ and $g_c = g_{\perp M2} = 2.00429$, while the experimental values were $g_a = g_b = 2.00761$ and $g_c = 2.00451$. Since $g_{\perp M1}$ (2.01059) is almost identical to g_x (2.01060), the N−O bond axis is thought to align nearly parallel to the cell plane in the crystalline phase of (*S*,*S*)-**1** (Figure 5c).

Conclusions

We examined the orientation of paramagnetic LC molecules **1** in a surface-stabilized LC cell by means of EPR spectroscopy. The angular dependence of the *g*-value has been explained by

the orientation models for each phase. We determined the molecular *g*-values ($g_{||M}$ and $g_{\perp M}$) in the molecular long axis frame by the Haller fitting of the temperature dependence of the *g*-value of (±)-**1** in the N phase. The observed coincidence between g_{ave} and g_{iso} indicates that no orientational polarization exists, which is most likely due to the surface stabilization effect on the cell surface prevailing over the effect of the magnetic field. On the other hand, we calculated $g_{||M}$ and $g_{\perp M}$ by conducting a coordinate transformation on a set of experimental principal *g*-values of the analogous nitroxide **2** into the molecular long axis frame while considering the structure of the LC molecule **1** calculated by MM3. The $g_{||M}$ and $g_{\perp M}$ values by both approaches are identical. Thus far, there has been no example of the study of the orientation of LC molecules in a surface-stabilized LC cell by EPR spectroscopy. As shown in this article, the method described in this work is effective for the determination of the orientation of LC molecules. We believe that this method will provide further important information on the orientation of various LC phases.

Acknowledgment. We thank Y. Iima (JEOL Co., Ltd.) for his support and advice regarding the construction of an EPR system specialized for the measurement of the LC cell sample.

Supporting Information Available: Mathematical derivation of the *g*-tensor for the N phase of (±)-**1** and the N* and crystalline phases of (*S,S*)-**1** (PDF). This material is available free of charge via the Internet at http://pubs.acs.org.

References and Notes

(1) Serrano, J. L., Ed. *Metallomesogens: Synthesis, Properties, and Applications*; VCH: Weinheim, 1996.

(2) Bikchantaev, I.; Gatyametdinov, Yu.; Prosvirin, A.; Griesar, K.; Soto-bustamante, E. A.; Haase, W. *Liq. Cryst.* **1995**, *18*, 231.

(3) Alonso, P. J.; Sanjuan, M. L.; Romero, P.; Marcos, M.; Serrano, J. L. *J. Phys.: Condens. Matter* **1990**, *2*, 9173.

(4) Hoshino, N.; Kodama, A.; Shibuya, T.; Matsunaga, Y.; Miyajima, S. *Inorg. Chem.* **1991**, *30*, 3091.

(5) Ikuma, N.; Tamura, R.; Shimono, S.; Kawame, N.; Tamada, O.; Sakai, N.; Yamauchi, J.; Yamamoto, Y. *Angew. Chem., Int. Ed.* **2004**, *43*, 3677.

(6) Haller, I. *Prog. Solid State Chem.* **1975**, *10*, 103.

(7) Manjuladevi, V.; Madhusadana, N. V. *Curr. Sci.* **2003**, *85*, 1056.

(8) Noda, Y.; Shimono, S.; Baba, M.; Yamauchi, J.; Uchida, Y.; Ikuma, N.; Tamura, R. *Appl. Magn. Reson.*, submitted.

(9) Chion, B.; Thomas, M. *Acta Crystallogr.* **1975**, *B31* (2), 472.

(10) Capiomont, A.; Chion, B.; Lajzerowicz, J. *J. Chem. Phys.* **1974**, *60*, 2530.

(11) Kikuchi, O. *Bull. Chem. Soc. Jpn.* **1969**, *42*, 47.

(12) Kikuchi, O. *Bull. Chem. Soc. Jpn.* **1969**, *42*, 1187.

(13) Kawamura, T.; Matsunami, S.; Yonezawa, T.; Fukui, K. *Bull. Chem. Soc. Jpn.* **1965**, *38*, 1935.

(14) Kawamura, T.; Matsunami, S.; Yonezawa, T. *Bull. Chem. Soc. Jpn.* **1967**, *40*, 1111.